Soft Matter

Accepted Manuscript

ROYAL SOCIETY OF CHEMISTRY

www.rsc.org/softmatter

Internal Organization of Macromonomers and Dendronized Polymers based on Thiophene Dendrons

Esther Córdova-Mateo,[1,2] Oscar Bertran,[1] A. Dieter Schlüter,[3] Martin Kröger,[3] and Carlos Alemán[2,4,*]

[1] Departament de Física Aplicada, Escola d'Enginyeria d'Igualada, Universitat Politècnica de Catalunya, Pça Rei 15, Igualada 08700, Spain

[2] Departament d'Enginyeria Química, E. T. S. d'Enginyeria Industrial de Barcelona, Universitat Politècnica de Catalunya, Diagonal 647, Barcelona E-08028, Spain

[3] Department of Materials, Institute of Polymers, Swiss Federal Institute of Technology, ETH Zurich, Vladimir-Prelog-Weg 5, 8093 Zurich, Switzerland

[4] Centre for Research in Nano-Engineering, Universitat Politècnica de Catalunya, Edifici C', C/Pasqual i Vila s/n, Barcelona E-08028, Spain

[*] carlos.aleman@upc.edu

ABSTRACT

The internal organization of macromonomers (MGs) consisting of all-thiophene dendrons of generation *g*= 2 and 3 attached to a phenyl core, as well as of the dendronized polymers resulting from polymerization of these macromonomers (PG2 and PG3, respectively), has been investigated using theoretical methods. The conformational preferences of the MGs, determined using density functional theory calculations, are characterized by the relative orientation between dendrons and core. We find that the strain of the MGs increases with the generation number and is alleviated by small conformational re-arrangements of the peripheral thiophene rings. The conformations obtained for the MGs have subsequently been used to construct models for the dendronized polymers. Classical molecular dynamics simulations have evidenced that the interpenetration of dendrons belonging to different repeat units is very small for PG2. In contrast, the degree of interpenetration is found to be very high for PG3, which also shows a significant degree of backfolding (*i.e.* occurrence of peripheral methyl groups approaching the backbone). Consequently, PG2 behaves as a conventional linear flexible polymer bearing bulk pendant groups, whereas PG3 is better characterized as a semirigid homogenous cylinder. The two polymers are stabilized by π-π stacking interactions, even though these are significantly more abundant for PG3 than for PG2; the average number of interactions per repeat unit is 3.0 and 8.8 for PG2 and PG3, respectively. While in these interactions the thiophene rings can adopt either parallel (sandwich) or perpendicular (T-shaped) dispositions, the former scenario turns out to be the most abundant.

INTRODUCTION

Organic molecules with dendritic architectures are typically classified in dendrimers and dendronized polymers (DPs). Dendrimers are the more widely investigated polymers[1-18] and consist of perfectly branched molecules made of tree-like fragments (dendrons) attached to a central core. The internal organization and size of these well-defined, often monodisperse, molecules depends on the generation number, *g*, of dendrons. Thus, dendrimers of lower generation have relatively loose inner structure while higher generations are densely packed and organized.[1-4] These particular organizations result in unusual properties, as for example liquid-crystalline behavior at high concentrations,[5,6] anomalous intrinsic viscosity,[7,8] and a multivalent molecular surface.[9,10] As a consequence, dendrimers have been proposed for very useful applications, as for example, drug-delivery systems,[11,12] gene vectors,[13,14] catalysts[15,16] and organic light-emitting diodes.[17,18]

DPs can be seen as wormlike macromolecular objects of cylindrical cross section.[19-21] The mass per repeat unit of the polymer backbone increases nonlinearly with the generation number (*g*), which allows to modulate properties like the rigidity, diameter and concentration of functionalities.[21-24] Due to this particular architecture, DPs currently represent a class of single molecular nanomaterials with several potential applications. Among the most promising applications of DPs are nanoscopic building blocks,[25,26] functional materials,[27,28] organic optoelectronic materials,[29,30] self-assembling vectors for complexation with DNA,[31,32] and nanomaterials to stabilize therapeutic proteins in the gastrointestinal tract[33] and both to copy[34] and to immobilize enzymes.[35] Furthermore, the structure of different families of DPs has been investigated using atomistic simulations, results providing microscopic understanding of the physical properties of these nanomaterials.[36-41] Importantly, these microscopic studies have

revealed that the internal organization and properties are intimately related not only with *g* but also with the chemical nature of the dendrons. For example, the stability of the right-handed helical conformation found for neutral and charged dendronized polymetylmethacrylates carrying chiral 4-aminoproline based dendrons is essentially due to the formation of networks of specific interactions.[36,37] In contrast, the interactions defined by the backfolding of the external dendrons dominates the properties of dendronized polymethacrylates made of tree-like fragments with amide and aromatic groups separated by polymethylenic segments.[38,39] These results supported the idea of treating these DPs as soft elongated colloidal objects.[40,41]

Thiophene (Th) based dendrimers and DPs with a fully π-conjugated core are considered as very promising kinds of conducting materials.[42] Since Advincula and co-workers reported on the first Th dendrimer synthesis,[43,44] several other Th dendrimers for different energy-related applications have been described.[42] For example, Bäuerle and co-workers[45] synthesized different all-Th dendrimers containing up to 90 Th rings with a divergent/convergent approach to facilitate the inclusion of functionalities in the external surface of the conducting dendrimer. These Th dendrimers were used as entangled photon sensors.[46] Mitchell *et al.*[47] prepared phenyl-cored Th dendrimers for organic photovoltaic devices, their power-conversion efficiency being recently overtaken by hexaperi-hexabenzocornene-cored Th dendrimers described by Wong *et al.*[48] and the hybrid gold-nanoparticle-cored dendrimers of Deng *et al.*[49] Furthermore, valuable microscopic and electronic information was derived from quantum mechanical studies on several Th-based dendrimers.[50-52]

In contrast, studies devoted to Th-based DPs are very scarce because of the intrinsic complexity associated to this kind of macromolecular objects. In a pioneering work, a few years ago Schlüter and co-workers[53] reported the synthesis of Th-containing second

and third generation dendronized macromonomers with methacrylate polymerizable units as well as their corresponding DPs. More recently, Kimura *et al.*[54] prepared novel all-Th dendritic macromonomers that were subsequently polymerized. The electronic and electrical properties of the resulting DPs, which showed enhanced conductivity upon doping, were attributed to the spatial overlapping of the Th dendrons through π-π interactions. Very recently, Griffin *et al.*[55] reported the synthesis and characterization of a benzodithiophene/Th alternating copolymers decorated with rigid, singly branched pendant side chains. Photoexcitation of these copolymers resulted in excited states primarily localized on the pendant side chains that excitations were rapidly transferred to the polymer backbone (*i.e.* in less than 250 fs).

In this work we use a multi-scale theoretical approach to characterize at the microscopic level the internal organization of macromonomers and DPs made of branched Th dendrons. More specifically, the molecular and electronic structures of two macromonomers, MG2 and MG3 in Figure 1a, have been studied using quantum mechanical methods based on density functional theory (DFT) calculations. After this, in a second step, DPs derived from the polymerization of MG2 and MG3 have been investigated using molecular dynamics (MD) simulations based on classical force-fields. The chemical structure of these DPs, named PG2 and PG3 (with g= 2 and 3, respectively), is depicted in Figure 1b. It is worth noting that MG2, MG3, PG2 and PG3 are practically identical to the macromonomers and their DPs synthesized by Schlüter and co-workers.[53] The only difference involves the alkyl groups attached to the Th rings, where we have replaced the hexyl groups of the experimental systems by methyl groups for simplicity.

METHODS

Quantum mechanical calculations.

All calculations were performed using the Gaussian 09 computer program.[56] The conformational preferences of MG2 and MG3 were examined using DFT calculations with the wB97X-D functional[57] combined with the 6-311+G(d,p) basis set,[58,59] (*i.e.* wB97X-D /6-311+G(d,p) level).

The ionization potential (IP) was estimated using the Koopman's theorem (KT),[60] according to which the IP was taken as the negative of the highest occupied molecular orbital (HOMO) energy (IP= $-\varepsilon_{HOMO}$). It is worth noting that KT is not applied to DFT methodologies since energies of Kohn-Shan orbitals do not involve any physical meaning. However, Janak's theorem[61] was used by Perdew[62] to show the connection between IP and the HOMO energy.

The lowest π-π^* transition energy (ε_g) was derived from the excitation energies calculated using time-dependent density functional theory (TD-DFT).[63] This methodology provides a robust and efficient description of the low-lying molecular states and is widely applied to study the UV-vis spectra of conjugated organic compounds.[64-66] Electronic excitations were evaluated using the PB0[67,68] and B3LYP[69,70] functionals, which are known to be very reliable for the calculation of electronic transitions,[71,72] combined with the 6-311+G(d,p) basis set and employing geometries fully optimized at the wB97X-D /6-311+G(d,p) level.

Electron densities of the most stable conformations identified for MG2 and MG3 were determined at the wB97X-D /6-311+G(d,p) level using the Merz-Kollman (MK) scheme,[73,74] which assigns point charges to fit the computed electrostatic potential to points on nested Connolly surface with a density of 1 point/Å^2.

Classical force field simulations.

The most stable structures of MG2 and MG3 obtained by DFT calculations were used to build the starting geometries for PG2 and PG3. The stability of the resulting structures was investigated in vacuum considering DP chains with N= 150 repeat units. Generally speaking, this solvent-free model corresponds to the situation encountered in the poor solvent experiments as was proved in previous studies of other non-charged DPs.[38,39] The backbone conformation of PG2 and PG3 was determined by applying a systematic search strategy. More specifically, 144 trial backbone conformations were constructed for each DP varying the dihedral angles α and β (Figure 1b) in steps of 30º. The number of backbone conformations without backbone–backbone, backbone–side group and side group–side group steric clashes, hereafter denoted *feasible* conformations, was approximately 30% and 20% of the initial trial conformation for PG2 and PG3, respectively. The rest of the conformations (*i.e.* those with atomic overlaps) were directly discarded without performing any calculation.

Energy minimizations and MD simulations of the feasible conformations were performed using the NAMD program.[75] The energy was calculated using the AMBER force-field.[76] All bonding and van der Waals parameters required for PG2 and PG3 were taken from the Generalized AMBER force-field[77] (GAFF) while atomic charges were computed at the wB97X-D /6-311+G(d,p) level using the Restrained ElectroStatic Potential (RESP) strategy (Figure 2).[78]

Geometry optimizations of all feasible conformations were performed by applying the conjugate gradient method during 5000 steps. After that, only 15% and 16% of feasible conformations were kept for PG2 and PG3, respectively. Such structures were pre-equilibrated by heating up the system from 0 to 298 K using a rate of 1 K each 1.5 ps. Visual inspection of the structures obtained after such short simulation time (*i.e.* 447 ps) indicated that many of them lost the initial helical regularity during the

thermalization process. Thus, only 6 and 4 configurations remained regular for PG2 and PG3, respectively. These structures were submitted to 5 ns of MD for equilibration. Finally, a 20 ns production ("relaxation") trajectory was carried out for the structure of lowest energy of each DP, which corresponds to that started using {α,β}= 180º, 60º and -150º,-60º for PG2 and PG3, respectively. Data were saved every 8 ps for subsequent analysis (*i.e.* 2500 snapshots).

Atom-pair distance cut-offs were applied at 14 Å to compute van der Waals and electrostatic interactions. Bond lengths involving hydrogen atoms were constrained using the SHAKE algorithm with a numerical integration step of 1 fs.[79] The temperature was controlled by a weak coupling method, the Berendsen thermostat[80] with a time constant for heat-bath coupling of 1 ps.

RESULTS AND DISCUSSION

MG2 and MG3 macromonomers

The conformational preferences of the dendron used to prepare MG2,[53] which consists of three Th rings linked by α-α and α-β linkages (3T; Scheme 1), was studied in a previous work.[52] More specifically, the potential energy surface derived from the systematic variation of the inter-ring dihedral angles was calculated at the B3LYP/6-31G(d) level. The most stable arrangement reported for 3T, with {ϕ,ϕ'}= 125º,-38º,[52] has been used in this work as starting point for the construction of MG2.

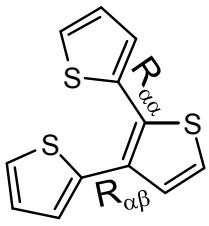

Scheme 1: Chemical structure of the dendron (3T) used to construct MG2

The conformational preferences of MG2 were calculated using a systemic strategy. For this purpose, after constructing the starting geometry, the potential energy surface defined by dihedral angles associated to the linkage between 3T and the phenyl core (θ and θ' in Figure 1a) was determined at the wB97X-D/6-311++G(d,p) level. Specifically, θ and θ' were varied between 0º and 360º in steps of 30º, the resulting 144 structures being optimized using a flexible rotor approximation (*i.e.* each structure was submitted to a constrained geometry optimization in which the inter-ring dihedral angles θ and θ' were kept fixed at their initial values).

Figure 3 displays the potential energy surface E=E(θ,θ') obtained for MG2, which was calculated without imposing any symmetry constraint. As it can be seen, the low-energy regions, which are indicated by blue colors in the map, are located at {θ,θ'}≈ ±30º,±150º, ±150º,±30º, ±150º,±150º and ±30º,±30º, where all combinations of signs are possible for each pair of values (*e.g.* {θ,θ'}≈ ±30º,±150º refers to the following four pairs: +30º,+150º; +30º,–150º; –30º,–150º; and –150º,–150º). The geometry of these 16 conformations was re-optimized without any constraint in θ and θ'. The dihedral angles and relative energies of the completely optimized representative conformations are displayed in Table 1. It should be pointed out that, although the four minima obtained for each pair of {θ,θ'} values are not formally equivalent because of the lack of molecular symmetry (Figure 1a), they are very similar in terms of energy and geometric properties. Accordingly, only one of four minima detected for each {θ,θ'} pair (that of lowest energy) has been explicitly included in Table 1. On the other hand, as the dihedrals ϕ and ϕ', which refer to the α-α and α-β linkages of the two peripheral Th rings to the central one (Figure 1a), are very similar for the two dendrons contained in MG2, Table 1 lists the average values and the corresponding standard deviations rather

than the explicit values for each dendron. Table 1 also includes the average values of α-α and α-β bond lengths (denoted $R_{\alpha\alpha}$ and $R_{\alpha\beta}$, respectively, in Scheme 1).

As it can be seen, the disposition of the peripheral Th rings is very similar for all conformations included in Table 1. This feature indicates that the two 3T dendrons used to prepare MG2 react upon the attachment to the phenyl core, provoking a significant conformational change in one of the peripheral Th rings. Thus, the conformation found for the individual 3T dendron, {ϕ,ϕ'}= 125º,-38º,[52] evolves towards {ϕ,ϕ'} ≈ 120º,140º. As occurred for {ϕ,ϕ'}, the $R_{\alpha\alpha}$ and $R_{\alpha\beta}$ values obtained for the different optimized conformations do not show appreciable differences. These observations are consistent with the very low relative energies (ΔE) separating the 16 optimized conformations, the energy gap between the most and the least stable conformation being of only 0.6 kcal/mol. The scarce influence of {θ,θ'} values on the relative stability and geometries facilitates the study and interpretation of MG2 properties, which have been analyzed for the lowest energy conformation only (MG2-1 in Table 1).

In the MG2-1 (Figure 4a) repulsive S···S interactions involving the Th rings directly attached to the phenyl core are strictly minimized by the dihedrals θ,θ'= 144.9º,-147.7º. The ε_g and IP values calculated at the PB0/6-311+G(d,p) and B3LYP/6-311+G(d,p) levels for such conformation, which are practically identical to those obtained the rest of minimized conformations, are in excellent agreement (*i.e.* ε_g= 3.65 eV and IP= 5.76 eV at the former level, and ε_g= 3.48 eV and IP= 5.56 eV at the latter level). The ε_g values derived from TD-DFT calculations slightly overestimate the experimental estimation, 3.00 eV, which was determined by absorption and emission spectroscopy.[53] However, our ε_g estimates are significantly lower than the value calculated for the individual 3T dendron (*i.e.* the theoretical ε_g obtained using DFT calculations at the B3LYP/6-31G(d) level for 4.13 eV[52] while the experimental measure was 3.33 eV[81]), which is fully

consistent with experimental observations. On the other hand, the IP predicted for MG2 by the KT, 0.97 eV per thiophene ring, is lower than that obtained at the B3LYP/6-31G(d) for the individual 3T dendron (*i.e.* 3.21 eV per thiophene ring).[52] Inspection of the topology of the highest occupied molecular orbital (HOMO) and the lowest unoccupied molecular orbital (LUMO), which are displayed in Figures 4b and 4c, evidences that these frontier orbitals are distributed through the aromatic rings of the two 3T dendrons and the phenyl core. This is fully consistent the homogeneous distribution of the electron density displayed in Figure 4d.

The conformational preferences of MG3 were evaluated using the following strategy. The four structures of lower energy identified in a previous study for the all-thiophene dendron used to prepare MG3, which has been denoted 7T (Scheme 2),[52] were attached to the phenyl core considering the following pairs of values for the dihedral angles θ,θ': 150º,-150º; 150º, 30º; 30º, 30º; and 30º,-150º. The 4×4= 16 starting structures were subjected to complete geometry optimization at the wB97X-D/6-311++G(d,p) level, resulting in 12 different conformations. Interestingly, the structures with θ,θ'≈ 150º,-150º are not stable when the generation number *g* increases from 2 to 3, reverting in conformations similar to those achieved after optimize the starting points with θ,θ'≈ 30º,-150º.

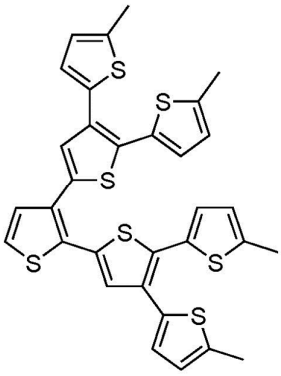

Scheme 2 Chemical structure of the dendron (7T) used to construct MG3

The three conformations of lower energy, which are listed in Table 2, are separated by an energy gap of 0.2 kcal/mol only, whereas the relative energy of the remaining optimized structures (not shown) was higher than 0.5 kcal/mol. The most stable conformation (G3-1 in Table 2) is displayed in Figure 4a. As occurred for MG2-1, S···S repulsive interactions are minimized in MG3-1. Also, Table 3 reflects that the strain of the macromonomer increases the generation number *g*. In order to alleviate such strain, inter-ring dihedral angles of different dendrons present larger deviations than in MG2, as is evidenced by the standard deviations of the corresponding averages. In spite of this, it is worth noting that the disposition of the peripheral Th rings is similar for MG2 and MG3, the dihedrals {ϕ,ϕ'} of the minima identified for each macromonomer differing in ~10º only.

The ε_g values derived for MG3-1 from TD-DFT calculations at the PB0/6-311+G(d,p) and B3LYP/6-311+G(d,p) levels are 3.50 and 3.31 eV, respectively. which represents a slight reduction with respect to MG2-1. This is fully consistent with the ε_g values experimentally determined for MG2 and MG3, which reflected a reduction of 0.35 eV.[53] The HOMO extends over two dendrons located of the same branch (Figure 4b), which represents a difference with respect to MG2-1. This provokes a slight reduction in the predicted IP values, which are 5.62 and 5.42 eV at the PB0/6-311+G(d,p) and B3LYP/6-311+G(d,p) levels, respectively. In contrast, the delocalization of the LUMO (Figure 4c) is similar to that observed for MG2-1. As occurred for MG2, the electron density is homogeneously distributed through the whole molecule (Figure 4d).

PG2 and PG3 dendronized polymers: Structural characterization

The conformational search strategy explained in the Methods section was applied to PG2 and PG3 chains made of N= 150 repeat units. Figure 5 represents a complete view of the final atomistic conformations obtained for PG2 and PG3 at the end of the MD production phase as well as details on both the backbone conformation and the inter-dendron interactions.

Table 3 displays the values of the average end-to-end distance, L_{av}, and the radius, R, derived from MD simulations for PG2 and PG3. As it can be seen, the chain length of the two DPs differs in ~100 Å, even though the same number of repeat units was considered in both cases. This should be attributed to the backbone flexibility, which is significantly higher for PG2 than for PG3. Analysis of the recorded snapshots evidences that, as the interpenetration of dendrons belonging to different repeat units is practically null in PG2, the backbone undergoes some irregularities (*e.g.* kinks and folds) (Figure 5, left) provoking a reduction of the molecular length. Thus, the conformational behavior of PG2 resembles that of a conventional linear flexible polymer bearing bulk pendant groups. In contrast, the interpenetration of dendrons belonging to different repeat units is very significant in PG3, which results in a significant degree of backbone stiffness (Figure 5, right). Thus, PG3 molecules can be viewed as semirigid homogenous cylinders. Similar features were obtained for bottle-brush polymers with high grafting density.[82-85] More specifically, the backbone end-to-end distance of bottle-brush macromolecules in solution and, especially, adsorbed onto surfaces was found to increase with growing length of the side chains, which was attributed to the fact that side chains progressively repel and stretch the backbone into an extended conformation. However, in DPs steric repulsions are provoked not only by the size of the side chains but also bytheir particular architectures, which promote interpenetration (see below).

In order to provide a quantitative estimation of the differences between the two DPs, interpenetrations have been defined as intertwined dendrons with uncrossability constraints. Accordingly, interpenetrations have been quantified through a geometric descriptor defined as the number of dendron – dendron crossing in a regular 2D projection of the DP chain averaged over all possible projections and calculated on the recorded snapshots. Thus, this geometric descriptor explains the occurrence of entanglements (*i.e.* overcrossings) that cause geometrically constrained motion in PG3. The mean number of dendron – dendron overcrossings is 23±10 and 108±16 for PG2 and PG3, respectively. These structural differences explain the drastic enlargement of the end-to-end distance experienced by PG3 with respect to PG2.

The radius *R* of each DP was determined considering a proportionality between the radial probability distribution and radial density profiles, $p(r) \propto \rho(r)$, and that the density profile, before it approaches zero is approximately constant as for a homogeneous cylinder of yet unspecified radius *R*. This case satisfies $p(r) \approx 1/r^2$ subject to normalization, $\int_0^R p(r)\,dr^2 = 1$, with $dr^2 = 2rdr$, and thus

$$\left\langle r^2 \right\rangle^{1/2} = \frac{R}{\sqrt{2}} \approx 0.71 \times R \qquad (1)$$

Although the persistence length of flexible PG2 cannot be derived from the present atomistic simulations due to the limited length of the model, cylindrical tracts are representative enough to obtain *R* values comparable to those calculated for PG3. As it was expected, *R* increases with increasing *g*. Thus, the thickness is 6.6 Å larger for PG3 than for PG2.

Figure 6a represents the variation of the density as function of radial distance *r* from the macromolecular backbone (MB) for PG2 and PG3, obtained by averaging over different cylindrical cross-sections of these macromolecules, while the average values

of the density (ρ_{av}) are listed in Table 3. It is worth noting that the density profiles reflect all the effects associated with the influence of *g* on the spatial distribution of the atoms (*e.g.* changes in backbone conformation). Figure 6a indicates that for PG2 the highest density is localized at the region close to the backbone, reaching a value of ~1.6 g/cm^3. After this, the density of PG2 fluctuates between 1.4 and 1.1 g/cm^3 due to conformational irregularities previously mentioned and, finally, it decreases progressively. For PG3 the density remains relatively constant from the backbone to a distance of approximately 9.9 Å and, hereafter, decreases slowly until the external layer of the cylinder section is reached. As it can be seen in Table 3, ρ_{av} is around 1 g/cm^3 for both DPs.

Figure 6b depicts the radial probability distribution of the peripheral methyl groups (see Figure 1b) as a function of the distance from the MB, $g_{\text{Me-b}}(r)$, for the two examined DPs. PG2, whose repeat unit presents two external dendrons, shows a single wide peak centered at around 12.9 Å, which corresponds to the value of *R* listed in Table 3. The peak observed for PG3, centered at approximately 17.3 Å, is smaller and broader than that observed for PG2. In addition of the position of the peak, which is located at a distance 2.2 Å smaller than *R* (Table 3), the $g_{\text{Me-b}}$ profile calculated for PG3 shows inner and outer tails. The inner tail is related with the backfolding or looping phenomenon, which refers to the probability of a peripheral methyl groups to be located at distances lower than *R*= 19.5 Å. For PG3 the broad inner tail indicates that some peripheral methyl groups are very close to the MB (~4 Å) and, therefore, evidencing that there must be parts of the same dendron residing at larger radial distances. In contrast, for PG2 the shape of the $g_{\text{Me-b}}$ profile indicates that the backfolding is practically null, the wideness of the peak being essentially due to the conformational flexibility of the backbone.

π-π Stacking interactions in PG2 and PG3

In a recent study we examined intramolecular and intermolecular interactions in DPs composed of a poly(methacrylic acid) backbone and repeat units with regularly branched dendrons of generation four containing amide and aromatic groups separated by a flexible segment (Scheme 3).[40] After analyzing several complexes formed by two interacting macromolecular chains, we concluded that intramolecular interactions are significantly more abundant than intermolecular ones. Thus, this DP forms rigid cylindrical-like molecules stabilized by intramolecular N–H···O hydrogen bonds and π-π stacking interactions between two aromatic rings arranged in a sandwich or T-shaped configuration, intermolecular interactions being only detected when two molecules interpenetrate considerably. The results supported the scenario put forth in previous structural and rheological studies,[23,41] which evidenced the colloidal-filament nature and associated solid-like viscoelastic response in the melt of such DP

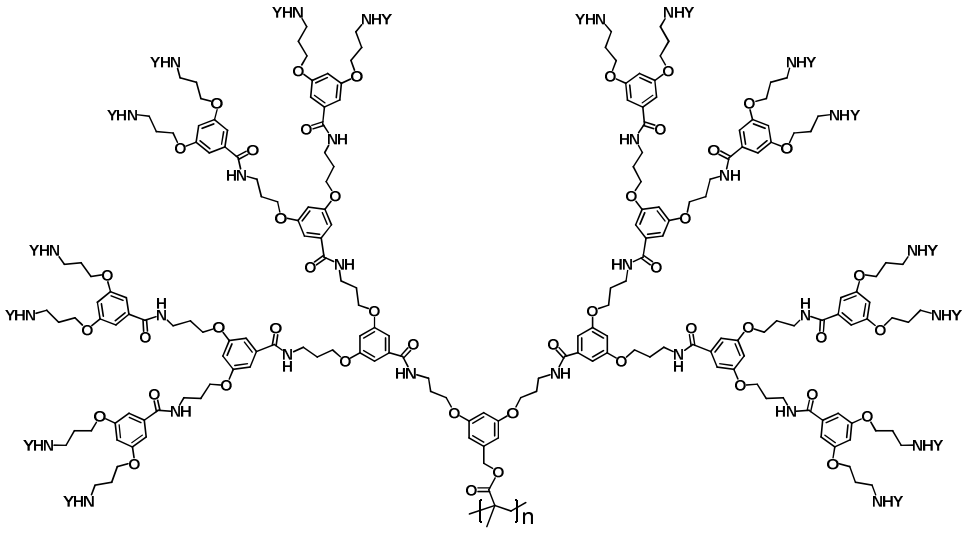

Scheme 3: Chemical structure of the DP with *g*= 4 studied in reference 40.

In an earlier study, the helical arrangement identified for the DP obtained from the spontaneous polymerization of a chiral 4-aminoproline-based second generation macromonomer (Scheme 4) was found to be stabilized by intramolecular hydrogen bonding networks that extend along the whole polymer chain.[36,37] Thus, the NH groups of the 4-aminoprolines were found to form this kind of interaction with the amide oxygen atoms of either the neighbor or the same repeat unit, enhancing the stability and stiffness of the right-handed helical conformation.

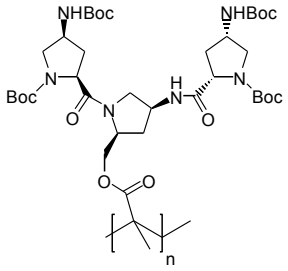

Scheme 4: DP studied in references 36 and 37.

According to these antecedents, intramolecular interactions are also expected to play a fundamental role in the stability of PG2 and PG3. Based on the molecular details given in Figure 1b, the only specific interactions that may exhibit the two DPs examined in this work correspond to the π-π-stacking of Th rings. The presence of these interactions is clearly reflected in Figure 7, which represents the partial radial distribution function for pairs of centers of masses of Th rings, $g_{\text{Th-Th}}(r)$. The very narrow and sharp peaks at r= 3.7, 4.1 and 4.8 Å (see insets) reflect the three inter-ring distances at 3T units (Scheme 1) contained in the side groups of both PG2 and PG3. Some other relatively narrow and sharp peaks are detected for PG2 at r= 7.3, 8.8 and 10.9 Å, which also correspond to regular distributions of 3T units. This is fully consistent with the absence of backfolding in PG2. The shoulder and the small peak centered at 4.4 and 5.2 Å (marked with arrows in Figure 7a), respectively, has been

attributed to two different types of π-π stacking interactions. More specifically, the shoulder at r= 4.4 Å has been attributed to π-π interactions in which the two aromatic rings are coplanar (sandwich configuration) while the two Th rings are perpendicular (T-shaped configuration) in the interaction associated to the peak at r=5.2 Å.[82]

In order to count the number of interactions of each type in PG2, the following cutoffs were considered. For the sandwich configuration the separation between the two Th rings (D in Scheme 5) is ≤ 4.5 Å and the degree of tilting (φ_d in Scheme 5) is < 45º or > 135º, whereas for the T-shaped configuration D ≤ 5.5 Å and φ_d ranges from 45º to 135º. Results obtained from all the snapshots saved during the production run, which are included in Table 3, indicate that the sandwich configuration is 3.4 times more frequent than the T-shaped one in PG2. Accordingly, the average number of π-π interactions per repeat unit of PG2 is 3 (*i.e.* 2.3 and 0.7 participate in sandwich and T-shaped configurations, respectively).

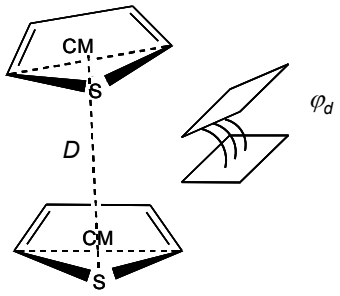

Scheme 5: Parameters used to define the sandwich and T-shaped configurations

The $g_{\text{Th-Th}}$ profile calculated for PG3 show broad peaks at r= 6.5, 7.8 and 8.9 Å (Figure 7b), which represents a significant difference with respect to PG2. Thus, the regularity in the position of the Th rings is lost in PG3 due to the backfolding phenomenon discussed above. The shoulder and peak centered at 4.4 and 5.2 Å (marked with arrows in Figure 7b) have been related with π-π stacking interactions, as occurred

for PG2. Quantitative analysis indicates that the total number of π-π stacking interactions for PG3 is around three times higher than for PG2 (Table 3). Thus, the average number of interactions counted per repeat unit of PG3 is 8.8 (*i.e.* 6.4 and 2.4 participate in sandwich and T-shaped configurations, respectively). According to these values, the relative frequency of the sandwich configuration with respect to the T-shaped one is lower for PG3 (2.7 : 1) than for PG2 (3.4 : 1). This should be attributed to the interpenetration and backfolding phenomena discussed above, which restricts the ability of the dendrons to rearrange and adopt T-shaped configurations.

CONCLUSIONS

The potential energy surface E=E(θ,θ') calculated for MG2 reveals that the well-defined conformational preferences of the macromonomers are essentially defined by the relative orientation between the all-thiophene dendrons and the phenyl core. The disposition of the peripheral Th rings, which is associated to the dihedral angles ϕ and ϕ', is similar for MG2 and MG3. However, small re-arrangements at these dihedrals allow to alleviate the conformational strain, which increases with *g*. The calculated electronic properties indicate that both the ε_g and the IP decrease with increasing *g*, which is in good agreement with experimental observations.

Atomistic models of PG2 and PG3, which were constructed using the most favored conformations of MG2 and MG3, evidenced very different internal organizations. PG2 behaves as a flexible linear polymer bearing bulk side group while PG3 is a semirigid cylinder. The particular behavior of the latter, which affects the molecular length, is due to both the interpenetration of dendrons belonging to different repeat units and presence of backfolding phenomena. In contrast, these effects are practically inexistent for PG2.

The different behaviors of PG2 and PG3 also affect the radial density profiles. The more uniform profile is obtained for PG3.

Analysis of the inter-dendron interactions in PG2 and PG3 reveals that π-π stacking interactions are significantly more abundant for latter than for the former. This is consistent with the semirigidity and backfolding of PG3 and the flexibility of PG2. Deeper analysis reveals that the interacting Th rings prefer the sandwich configuration with respect to the T-shaped one, this effect being more pronounced for PG2 than PG3.

ACKNOWLEDGEMENTS

Financial support from the MINECO and FEDER (MAT2012-34498) and Generalitat de Catalunya (Research group 2009 SGR 925 and XRQTC) is gratefully acknowledged. EC-M is thanked for the financial support through a FPI grant.

REFERENCES

1. G. R. Newkome and C. Shreiner, C., *Chem. Rev.*, 2010, **110**, 6338-6442.

2. M. Ballauff and C. N. Likos, *Angew. Chem., Int. Ed.*, 2004, **43**, 2998-3020.

3. P. K. Maiti, T. Cagin, G. Wang and W. A. Goddard III, *Macromolecules*, 2004, *37*, 236-6254.

4. Y. Liu, C. Y. Chen, H. L. Chen, K. L. Hong, C. Y. Shew, X. Li, L. Liu, Y. B. Melnichenko, G. S. Smith, K. W. Herwig, L. Porcar and W. R. Chen, *J. Phys. Chem. Lett.*, 2010, **1**, 2020-2024.

5. X. F. Li, T. Imae, D. Leisner and M. A. Lopez-Quintela, *J. Phys. Chem. B*, 2002, **106**, 12170-12177.

6. R. Mezzenga, J. Ruokolainen, N. Canilho, E. Kasemi, A. D. Schlüter, W. B. Lee and G. H. Fredrickson, *Soft Matter*, 2009, **5**, 92-97.

7. Y. Lu, T. Shi, L. An, L. Jin and Z.-G. Wang, *Soft Matter*, 2010, **6**, 2619-2622

8. T. H, Mourey, S. R. Turner, M. Rubinstein, J. M. J. Frechet, C. J. Hawker and K. L. Wooley, *Macromolecules*, 1992, **25**, 2401-2406.

9. D. Astruc, E. Boisselier and C. Ornelas, *Chem. Rev.*, 2010, **110**, 1857-1959.

10. G. R. Newkome, C. N. Moorefield and F. Vögtle, Dendrimers and Dendrons: Concepts, Syntheses, Applications, Wiley-VCH, Weinheim, Germany, 2001.

11. A.-M. Caminade and C.-O. Turrin, *J. Mater. Chem. B*, 2014, **2**, 4055-4066.

12. G. M. Soliman, A. Sharma, D. Maysinger and A. Kakkar, *Chem. Commun.*, 2011, **47**, 9572-9587.

13. N. K. Voulgarakis, K. O. Rasmussen and P. M. Welch, *J. Chem. Phys.*, 2009, **130**, 155101.

14. H. M. Liu, Y. Wang, M. M. Wang, J. R. Xiao and Y. Y. Cheng, *Biomaterials*, 2014, **35**, 5407-5413.

15. L. Ropartz, R. E. Morris, D. F. Foster and D. J. Cole-Hamilton, *Chem. Commun.*, 2001, 361-362.

16. E. Karakhanov, A. Maximov, Y. Kardasheva, V. Semernina, A. Zolotukhina, A. Ivanov, G. Abbott, E. Rosenberg and V. Vinokurov, *ACS Mater. Interfaces*, 2014, **6**, 8807-8816.

17. J. Y. Li, Q. Li and D. Liu, *ACS Mater. Interfaces*, 2011, **3**, 2099-2107.

18. J. Y. Li, T. Zhang, Y. J. Liang and R. X. Yang, *Adv. Funct. Mater.*, 2013, **23**, 619-628.

19. A. D. Schlüter and J. P. Rabe, Angew. *Chem., Int. Ed.*, 2000, **39**, 864-883.

20. B. M. Rosen, C. J. Wilson, D. A. Wilson, M. Peterca, M. R. Imam and V. Percec, *Chem. Rev.*, 2009, **109**, 6275-6540.

21. Y. Guo, J. D. van Beek, B. Zhang, M. Colussi, P. Walde, A. Zhang, M. Kröger, A. Halperin and A. D. Schlüter, *J. Am. Chem. Soc.*, 2009, **131**, 11841-11854.

22. B. Zhang, R. Wepf, K. Fischer, M. Schmidt, S. Besse, P. Lindner, B. T. King, R. Sigel, P. Schurtenberger, Y. Talmon, Y. Ding, M. Kröger, A. Halperin and A. D. Schlüter, *Angew. Chem. Int. Ed.*, 2011, **50**, 763-766.

23. A. Kroeger, B. Zhang, C. Rosenauer and A. D. Schlüter, *Colloid Polym. Sci.*, 2013, **291**, 2879-2892.

24. B. Zhang, R. Wepf, M. Kröger, A. Halperin and A. D. Schlüter, *Macromolecules*, 2011, **44**, 6785-6792.

25. Z. S. Bo, J. P. Rabe and A. D. Schlüter, *Angew. Chem. Int. Ed.*, 1999, **38**, 2370.

26. V. Percec, C. H. Ahn, T. K. Bera, G. Ungar, D. J. P. Yeardley, *Chem. Eur. J.*, 1999, **5**, 1070-1083.

27. C. O. Liang, B. Helms, C. J. Hawker and J. M. J. Frechet, *Chem. Commun.*, **2003**, 2524-2525.

28. B. M. J. M. Suijkerbuijk, L. J. Shu, R. J. M. K. Gebbink, A. D. Schlüter and G. van Koten, *Organometallics*, 2003, **22**, 4175-4177.

29. Z. N. Bao, K. R. Amundson and A. J. Lovinger, *Macromolecules*, 1998, **31**, 8647-8649.

30. T. Sato, D. L. Jiang and T. Aida, *J. Am. Chem. Soc.*, 1999, **121**, 10658-10659.

31. D. Joester, M. Losson, R. Pugin, H. Heinzelmann, E. Walter, H. P. Merkle and F. Diederich, *Angew. Chem. Int. Ed.*, 2003, **42**, 1486-1490.

32. I. Gossl, L. J. Shu, A. D. Schlüter and J. P. Rabe, *J. Am. Chem. Soc.*, 2002, **124**, 6860-6865.

33. G. Fuhrmann, A. Grotzky, R. Lukic, S. Matoori, P. Luciani, H. Yu, B. Zhang, P. Walde, A. D. Schlüter and J.-C. Leroux, *Nature Chem.*, 2013, **5**, 582-589.

34. A. Grotzky, T. Nauser, H. Erdogan, A. D. Schlüter and P. Walde, *J. Am. Chem. Soc.*, 2012, **134**, 11392-11395.

35. S. Fornera, T. E. Balmer, B. Zhang, A. D. Schlüter and P. Walde, *Macromol. Biosci.*, 2011, **11**, 1052-1067.

36. A. Zhang, F. Rodríguez-Ropero, D. Zanuy, C. Alemán, E. W. Meijer and A. D. Schlüter, *Chem. Eur. J.*, 2008, **14**, 6924-6934.

37. F. Rodríguez-Ropero, M. Canales, D. Zanuy, A. Zhang, A. D. Schlüter and C. Alemán, *J. Phys. Chem. B*, 2009, **113**, 14868-14876.

38. O. Bertran, B. Zhang, A. D. Schlüter, A. Halperin, M. Kröger and C. Aleman, *RSC Adv.*, 2013, **3**, 126-140.

39. O. Bertran, B. Zhang, A. D. Schlüter, M. Kröger and C. Alemán, *J. Phys. Chem. B*, 2013, **117**, 6007-6017.

40. E. Córdova-Mateo, O. Bertran, B. Zhang, D. Vlassopoulos, R. Pasquino, A. D. Schlüter, M. Kröger and C. Alemán, *Soft Matter*, 2014, **10**, 1032-1044.

41. R. Pasquino, B. Zhang, R. Sigel, H. Yu, M. Ottiger, O. Bertran, C. Aleman, A. D. Schlüter and D. Vlassopoulos, *Macromolecules*, 2012, **45**, 8813-8823.

42. A. Mishra, C. Q. Ma and P. Baeuerle, *Chem. Rev.*, 2009, **109**, 1141-1276.

43. C. Xia, X. Fan, J. Locklin and R. C. Advincula, *Org. Lett.*, 2002, **4**, 2067-2070.

44. C. Xia, X. Fan, J. Locklin, R. C. Advincula, A. Gies and W. Nonidez, *J. Am. Chem. Soc.*, **2004**, *126*, 8735-8743.

45. C.-Q. Ma, E. Mena-Osteritz, T. Debaerdemaeker, M. M. Wienk, R. A. Janssen and P. Bäuerle, *Angew. Chem. Int. Ed.*, 2007, **46**, 1679-1683.

46. M. R. Harpham, Ö. Süzer, C. Q. Ma, P. Bäuerle and T. Goodson III, *J. Am. Chem. Soc.*, 2009, **131**, 973-979.

47. W. J. Mitchell, N. Kopidakis, G. Rumbles, D. S. Ginley and S. E. Shaheen, *J. Mater. Chem.*, 2005, **15**, 4518-4528.

48. W. W. H. Wong, C. Q. Ma, W. Pisula, C. Yan, X. Feng, D. J. Jones, K. Müllen, R. A. J. Janssen, P. Bäuerle and A. B. Holmes, *Chem. Mater.* 2010, **22**, 457-466.

49. S. Deng, G. Fulghum, Krueger, D. Patton, Y. Park and R. C. Advincula, *Chem. Eur. J.*, 2011, **17**, 8929-8940.

50. E. Córdova-Mateo, F. Rodríguez-Ropero, O. Bertran and C. Alemán, *Chem. Phys. Chem.*, 2012, **13**, 1354-1362.

51. E. Badaeva, M. R. Harpham, R. Guda, O. Suzer, C. Q. Ma, P. Bäuerle, T. Goodson and S. Tretiak, *J. Phys. Chem. A*, 2010, **114**,15808-15817.

52. F. Rodríguez-Ropero, D. Zanuy and C. Alemán, *Polymer*, 2010, **51**, 308-315.

53. P. Sonar, H. Benmansour, T. Geiger and A. D. Schlüter, *Polymer*, 2007, **48**, 4996-5004.

54. M. Kimura, A. Kitao, R. Fukawa and H. Shirai, *Chem. Eur. J.*, 2011, **17**, 6821-6829.

55. G. B. Griffin, P. M. Lundin, B. S. Rolczynski, A. Linkin, R. D. McGillicuddy, Z. Bao and G. S. Engel, *J. Chem. Phys.*, 2014, **140**, 034903.

56. M. J. Frisch, G. W. Trucks, H. B. Schlegel, G. E. Scuseria, M. A. Robb, J. R. Cheeseman, G. Scalmani, V. Barone, B. Mennucci, G. A. Petersson, H. Nakatsuji, M. Caricato, X. Li, H. P. Hratchian, A. F. Izmaylov, J. Bloino, G. Zheng, J. L. Sonnenberg, M. Hada, M. Ehara, K. Toyota, R. Fukuda, J. Hasegawa, M. Ishida, T. Nakajima, Y. Honda, O. Kitao, H. Nakai, T. Vreven, J. A. Montgomery Jr., J. E. Peralta, F. Ogliaro, M. Bearpark, J. J. Heyd, E. Brothers, K. N. Kudin, V. N. Staroverov, R. Kobayashi, J. Normand, K. Raghavachari, A. Rendell, J. C. Burant, S. S. Iyengar, J. Tomasi, M. Cossi, N. Rega, J. M. Millam, M. Klene, J. E. Knox, J. B. Cross, V. Bakken, C. Adamo, J. Jaramillo, R. Gomperts, R. E. Stratmann, O. Yazyev, A. J. Austin, R. Cammi, C.

Pomelli, J. W. Ochterski, R. L. Martin, K.Morokuma, V. G. Zakrzewski, G. A. Voth, P. Salvador, J. J. Dannenberg, S. Dapprich, A. D. Daniels, O. Farkas, J. B. Foresman, J. V. Ortiz, J. Cioslowski and D. J. Fox, Gaussian 09, revision A.01, Gaussian, Inc., Wallingford, CT, 2009.

57. J. D. Chai and M. Head-Gordon*Phys. Chem. Chem. Phys.*, 2008, **10**, 6615-6620.

58. A. D. McLean and G. S. Chandler, *J. Chem. Phys.*, 1980, **72**, 5639-5648.

59. M. J. Frisch, J. A. Pople and J. S. Binkley, *J. Chem. Phys.*, 1984, **80**, 3265-3269.

60. T. Koopmans, *Physica*, 1934, **1**, 104-113.

61. J. D. Janak, *Phys. Rev. B*, 1978, **18**, 7165-7168.

62. R. M. Dreizler and J. da Providência, Density Functional Methods in Physics, Springer Dordrecht, 1985.

63. E. Runge and E. K. U. Gross, *Phys. Rev. Lett.*, 1984, **52**, 997-1000.

64. D. Jacquemin, J. Preat, E. A. Perpete and C. Adamo, *Int. J. Quatum Chem.*, **2010**, *110*, 2121-2129.

65. A. Laurent and D. Jacquemin, *Int. J. Quatum Chem.*, 2013, **113**, 2019-2039.

66. C. Adamo and D. Jacquemin, *Chem. Rev.*, 2013, **42**, 845-856.

67. J. P. Perdew, M. Ernzerhof and K. Burke, *J. Chem. Phys.* 1996, **105**, 9982-9985.

68. C. Adamo and V. Barone, *J. Chem. Phys.*, 1999, **110**, 6158-6170.

69. A. D. Becke, *J. Chem. Phys.* 1993, **98**, 5648-5652.

70. C. Lee, W. Yang and R. G. Parr, *Phys. Rev. B*, 1988, **37**, 785-789.

71. J. Torras, J. Casanovas and C. Alemán, *J. Phys. Chem. A*, 2012, **116**, 7571-7583.

72. D. Jacquemin, E. A. Perpete, I. Ciofini and C. Adamo, *Acc. Chem. Res.*, 2009, **42**, 326-334.

73. U. C. Singh and P. A. Kollman, *J. Comput. Chem.*, 1984, **5**, 129-145.

74. B. H. Besler, K. M. Merz and P. A. Kollman, *J. Comput. Chem.*, 1990, **11**, 431-439.

75. J. C. Phillips, R. Braun, W. Wang, J. Gumbart, E. Tajkhorshid, E. Villa, C. Chipot, R. D. Skeel, L. Kale and K. Schulten, *J. Comput. Chem.*, 2005, **26**, 1781-1802.

76. W. D. Cornell, P. Cieplak, C. I. Bayly, I. R. Gould, K. M. Merz, D. M. Ferguson, D. C. Spellmeyer, T. Fox, J. W. Caldwell and P. A. Kollman, *J. Am. Chem. Soc.*, 1995, **117**, 5179-5197.

77. J. Wang, R. M. Wolf, J. W. Caldwell and D. A. Case, *J. Comput. Chem.*, 2004, **15**, 1157-1174.

78. P. Cieplak, W. Cornell, C. I. Bayly and P. A. Kollman, *J. Comput. Chem.*, 1995, **16**, 1357-1377.

79. J. P. Ryckaert, G. Ciccotti and H. J. C. Berendsen, *J. Comput. Phys.*, 1977, **23**, 327-341.

80. H. J. C. Berendsen, J. P. M. Postma, W. F. van Gunsteren, A. Di Nola and J. R. Haak, *J. Chem. Phys.*, 1984, **81**, 3684-3690.

81. C. Xia, X. Fan, J. Locklin, R. C. Advincula, A. Gies and W. Nonidez, *J. Am. Chem. Soc.*, 2004, **126**, 8735-8743.

82. S. S. Sheiko, F. C. Sun, A. Randall, D. Shirvanyants, M. Rubinstein, H-I Lee and K. Matyjaszewski, *Nature*, 2006, **440**, 191-194.

83. A. Milchev, J. Paturej, V. G. Tostiashvili and T. A. Vilgis, *Macromolecules*, 2011, **44**, 3981.3987.

84. S. Panyukov, E. B. Zhulina, S. S. Sheiko, G. C. Randall, J. Brock, M. Rubinstein, *J. Phys. Chem. B*, 2009, **113**, 3750–3768

85. J. Paturej, L. Kuban, A. Milchev and T. A. Vilgis, *Eurphys. Lett.*, 2012, **97**, 58003.

86. F. Rodriguez-Ropero, J. Casanovas and C. Alemán, *J. Comput. Chem.*, 2008, **29**, 69-78.

CAPTIONS TO FIGURES

Figure 1. Chemical structure of: (a) MG2 and MG3 macromonomers; and (b) PG2 and PG3 DPs.

Figure 2. Electrostatic parameters determined for the repeat unit of (a) PG2 and (b) PG3. Charges in parenthesis correspond to hydrogen atoms, where $\times n$ refer to the number n of equivalent hydrogens, while charges for carbon, oxygen and sulfur atoms are out of the parenthesis. Charges for equivalent thiophene rings are omitted for clarity. In the repeat unit of PG3, equivalent pairs of thiophene rings have been labelled using letters.

Figure 3. Potential energy surface E=E(θ,θ') calculated for MG2. The dihedral angles θ and θ' are displayed in Figure 1a.

Figure 4. (a) Molecular representation, (b) HOMO, (c) LUMO and (d) electron density of the MG2-1 (left) and MG3-1 (right) structures.

Figure 5. Atomistic conformations for PG2 (left) and PG3 (right). The complete axial projections represent the whole calculated systems, the number of repeat units being N= 150. The magnified axial projection involves 20 repeat units in all cases, whereas the equatorial projection involves 10 repeat units.

Figure 6. (a) Density profile for PG2 and PG3 representing the density (ρ) against the distance to the backbone measured using the vector perpendicular to the helical axis (r). The profile displayed for each DP corresponds to an average considering different cross-sections within a given snapshot. (b) Distribution of peripheral methyl groups ($g_{Me\text{-}b}$) as a function of the distance from the backbone for PG2 and PG3. All data were obtained by averaging over 2500 snapshots taken during the last 20 ns of the MD relaxation runs.

Figure 7. Partial radial distribution functions for the pairs of centers of masses of Th rings of (a) PG2 and (b) PG3. Data in were obtained by averaging over 2500 snapshots taken during the last 20 ns of the MD relaxation runs.

Table 1. Representative minimum energy conformations calculated for MG2 at the wB97X-D/6-311++G(d,p) level. Dihedral angles (θ, θ', ϕ and ϕ'; in degrees), bond lengths ($R_{\alpha\alpha}$ and $R_{\alpha\beta}$; in Å) and relative energy (ΔE; in kcal/mol) are displayed.

#	θ	θ'	ϕ	ϕ'	$R_{\alpha\alpha}$	$R_{\alpha\beta}$	ΔE
MG2-1[a]	144.9	-147.7	118.9±0.4	141.2±0.6	1.461±0.000	1.463±0.002	0.0
MG2-2[b]	147.6	33.6	119.5±0.6	140.5±0.1	1.461±0.000	1.465±0.000	0.0
MG2-3[c]	34.5º	33.0	120.9±0.9	140.0±0.1	1.461±0.000	1.465±0.000	0.0
MG2-4[d]	31.1º	-148.5	119.3±0.4	142.2±0.8	1.461±0.000	1.465±0.000	0.2

[a] The ΔE of minima with θ,θ' = 144.9º,-147.7º; -147.9º,-146.1º; 147.6º,146.3º; and -145.9º,150.0º is lower than 0.2 kcal/mol. Differences in the rest of the geometric parameter are practically inexistent. [b] The ΔE of minima with θ,θ' = 147.6º,33.6º;-145.9º,-34.4º; -147.4º,33.2º; and 146.3º,-32.4º is lower than 0.2 kcal/mol. Differences in the rest of the geometric parameter are practically inexistent. [c] The ΔE of minima with θ,θ' = 34.5º,33.0º; 34.0º,-34.3º; -35.9º,31.8º; and -30.5º,-32.0º is lower than 0.6 kcal/mol. Differences in the rest of the geometric parameter are practically inexistent. [d] The ΔE of minima with θ,θ' = 34.1º,-148.5º; -36.2º,-148.3º; 35.2º,-147.9º; and -34.8º,-148.6º is lower than 0.4 kcal/mol. Differences in the rest of the geometric parameter are practically inexistent.

Table 2. Representative minimum energy conformations calculated for MG3 at the wB97X-D/6-311++G(d,p) level. Dihedral angles (θ, θ', ϕ and ϕ'; in degrees), bond lengths ($R_{\alpha\alpha}$ and $R_{\alpha\beta}$; in Å) and relative energy (ΔE; in kcal/mol) are displayed.

#	θ	θ'	ϕ	ϕ'	$R_{\alpha\alpha}$	$R_{\alpha\beta}$	ΔE
MG3-1	148.8	31.5	110.1±4.4	148.7±8.3	1.463±0.002	1.465±0.001	0.0
MG3-2	33.6	33.7	110.9±5.1	149.0±7.6	1.463±0.002	1.464±0.001	0.0
MG3-3	34.6º	-146.7	111.9±4.1	147.5±8.4	1.463±0.002	1.464±0.001	0.2

Table 3. Properties and interactions calculated by MD simulations for PG2 and PG3. Regarding to properties, L_{av}, R and ρ_{av} refer to the average end-to-end distance, the radius and the average density, respectively. Regarding to interactions, the average number of π-π stacking interactions with T-shaped and sandwich configurations in a polymer chain made of 150 repeat units are supplied.

	L_{av} (Å)	R (Å)	ρ_{av} (g/cm^3)	π-π Stacking T-shaped	π-π Stacking Sandwich
PG2	222±4	12.9±0.1	1.05	101±11	343±13
PG3	323±1	19.5±0.1	0.99	358±20	955±21

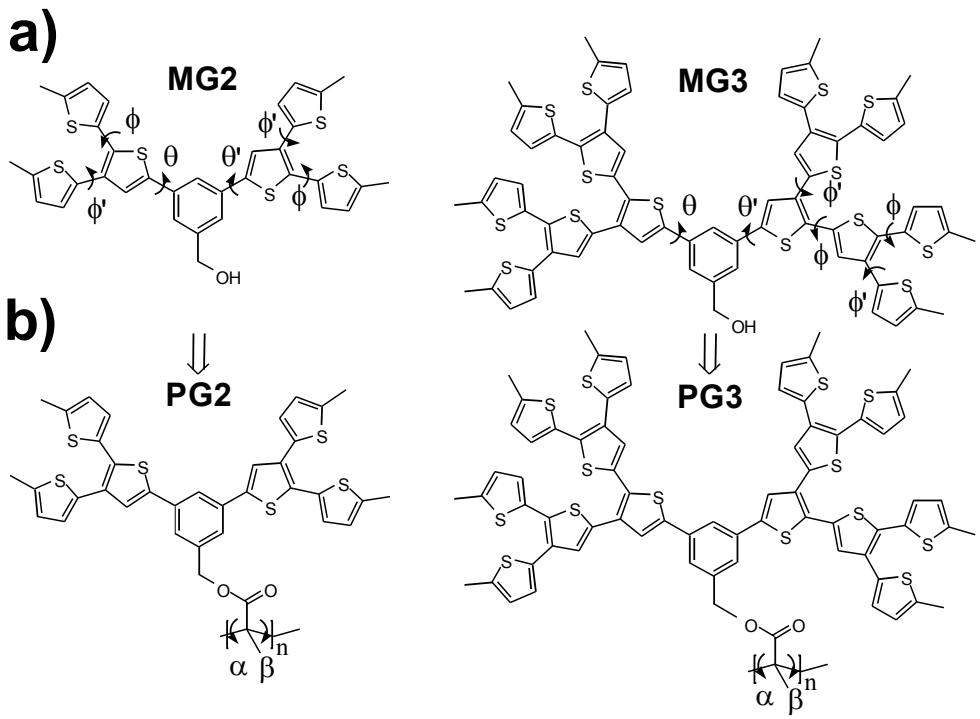

Figure 1

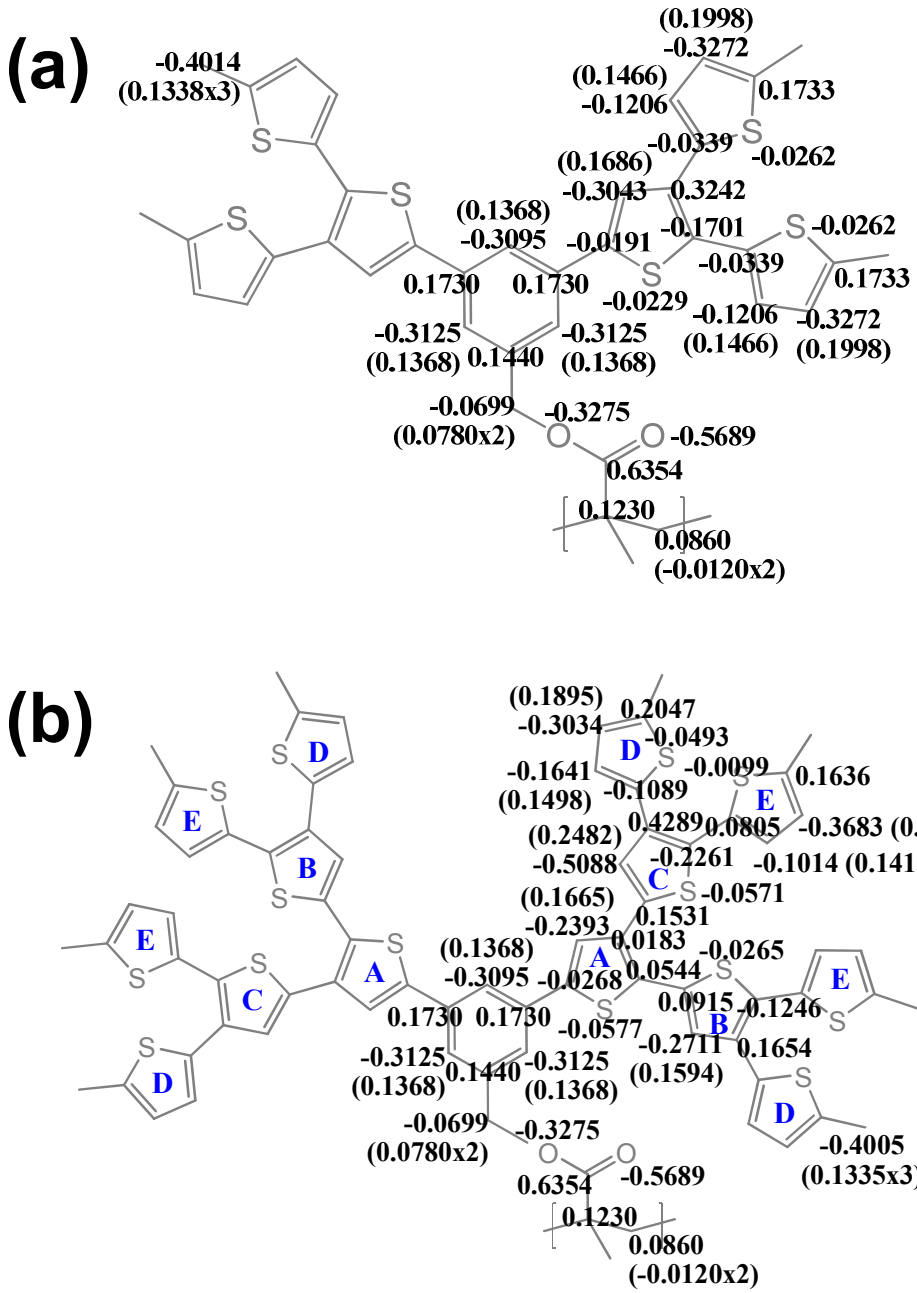

Figure 2

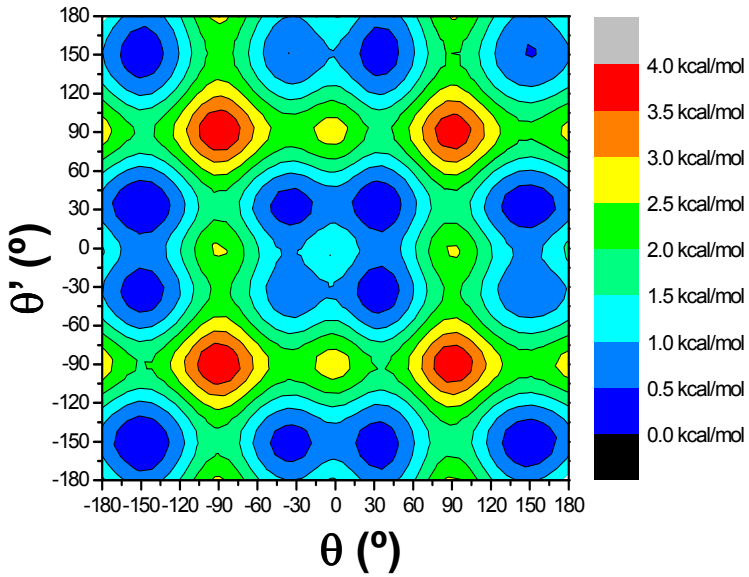

Figure 3

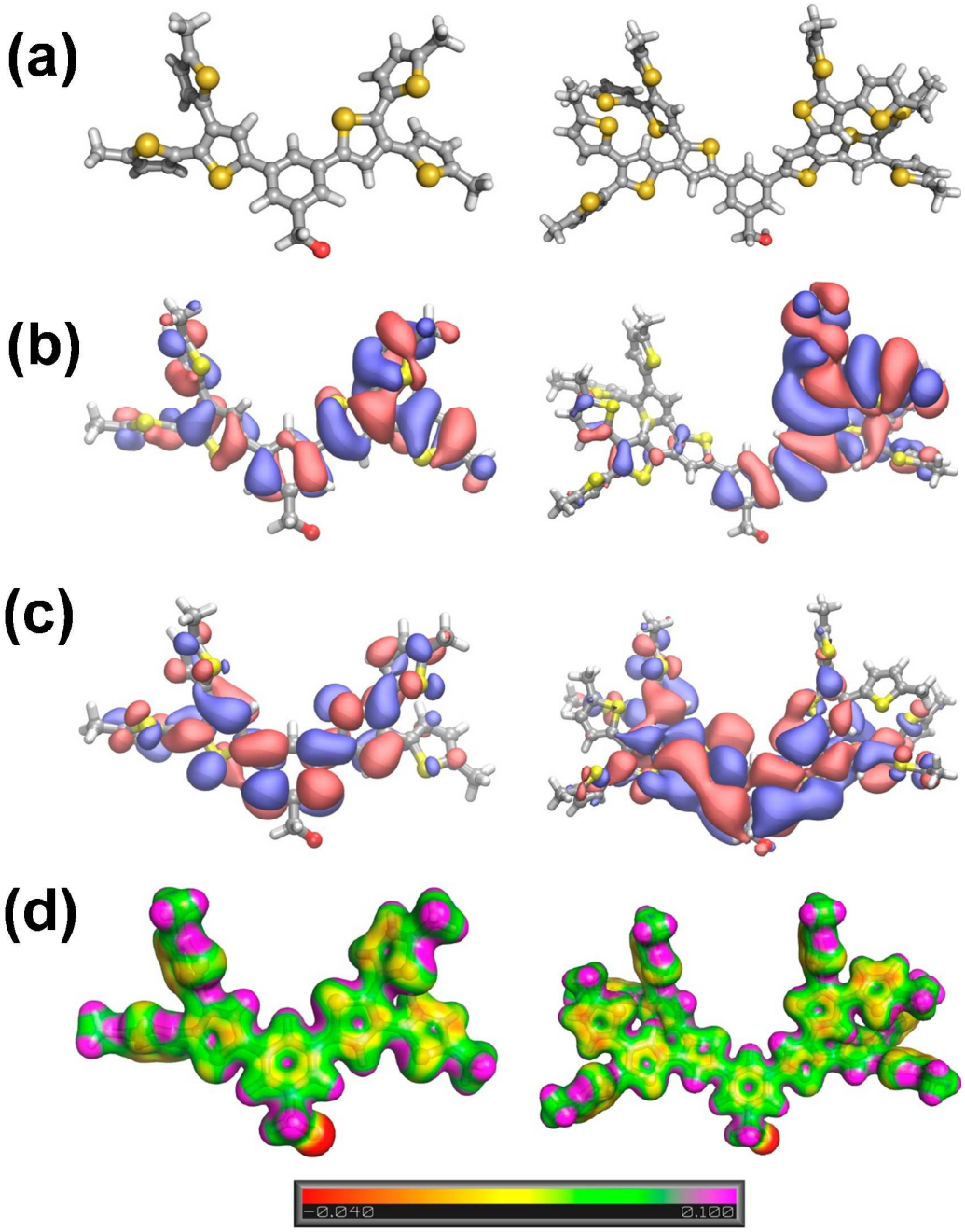

Figure 4

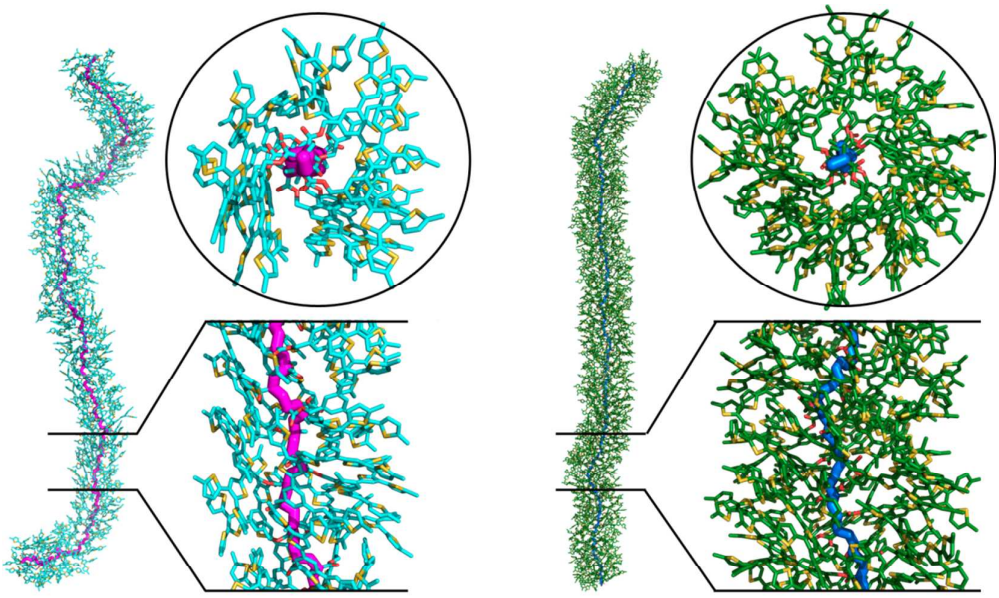

Figure 5

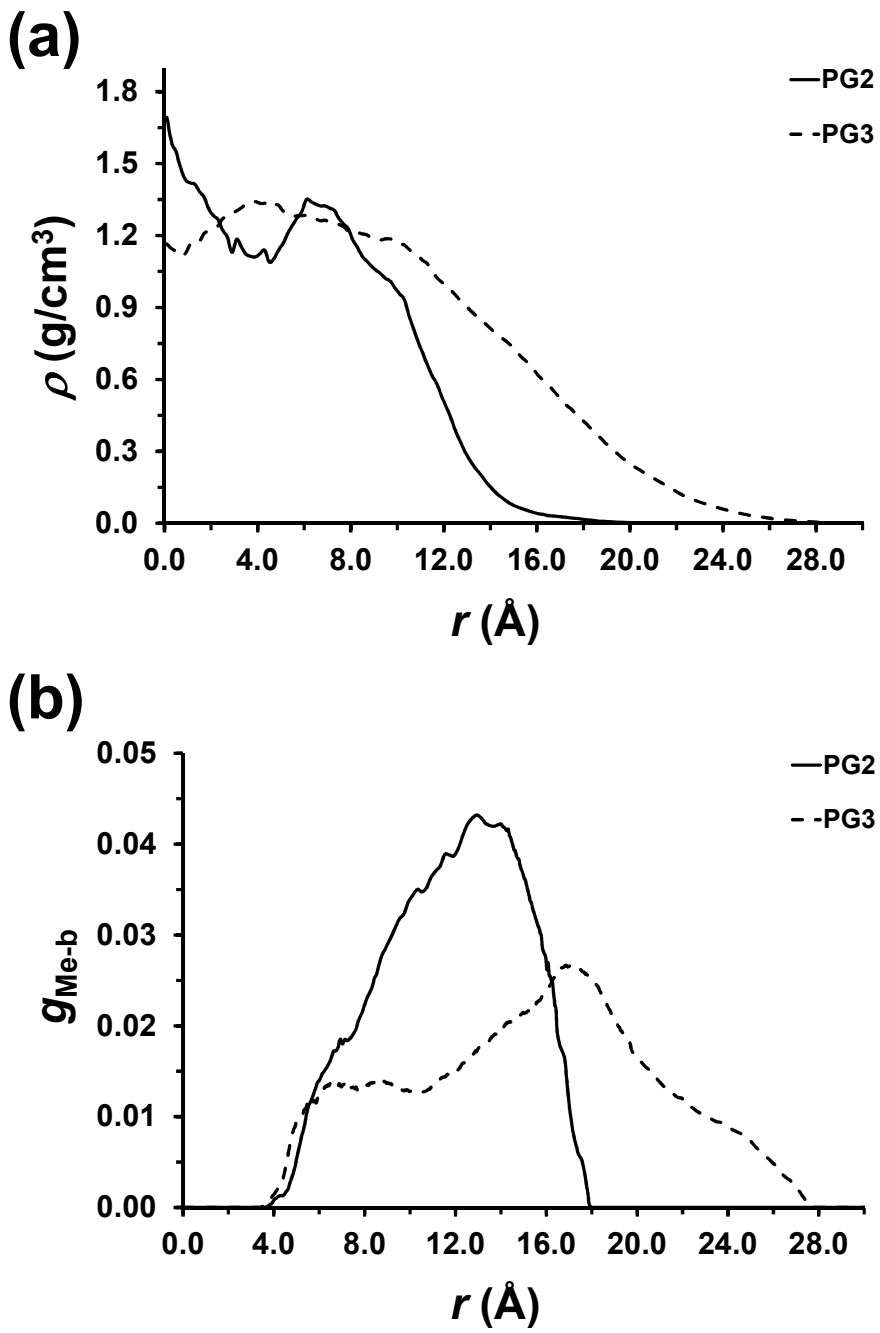

Figure 6

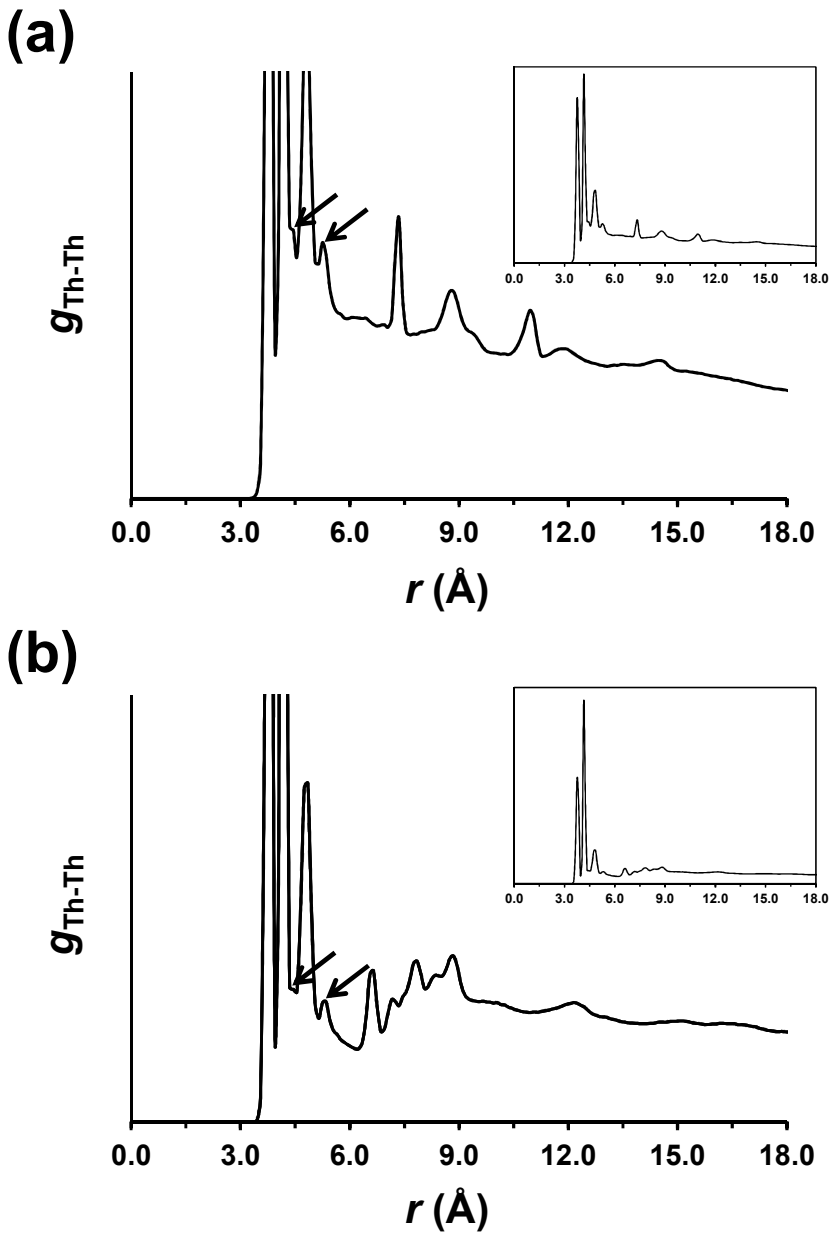

Figure 7

GRAPHICAL ABSTRACT

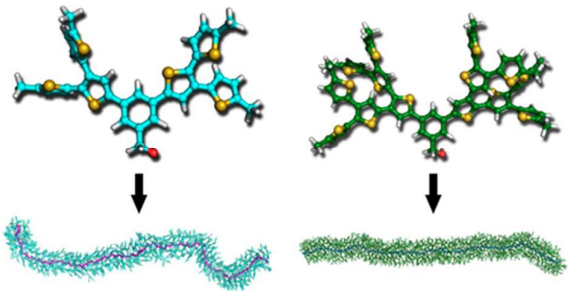

Multi-scale simulations reveal the organization of macromonomers and dendronized polymers derived from all-thiophene dendrons attached to a phenyl core